Spike-Timing Dependent Plasticity as a Mechanism for Ocular Dominance Shift

Beth Ann Siegler [a,1], Maureen Ritchey [b,1], Jonathan Rubin [c,1,2]

[a] *Center for Neuroscience, University of Pittsburgh, Pittsburgh, PA 15260*

[b] *University of Notre Dame, South Bend, IN 46556*

[c] *Department of Mathematics and Center for the Neural Basis of Cognition, University of Pittsburgh, Pittsburgh, PA 15260*

Abstract

Spike-timing dependent plasticity (STDP) has been implicated in visual cortex modification. We created a model of ocular dominance (OD) shift based on STDP rules and compared it to experimental results. Although STDP proved to be a powerful mechanism for OD shift in our model, we found that it was unable to account for more subtle effects of monocular deprivation.

Key words: Spike-timing dependent plasticity, ocular dominance, monocular deprivation, monocular inactivation

1 Introduction

The mammalian visual cortex features ocular dominance (OD) columns, each consisting of a group of cortical cells that preferentially respond to one eye; see Figure 1a. Depriving one eye of light (monocular deprivation, or MD) causes the OD columns corresponding to the non-deprived eye to expand, while deprived-eye OD columns shrink. Postsynaptic activity is necessary for OD shift [13], consistent with Hebbian learning, but the mechanisms through which OD shift occurs remain unclear.

Rittenhouse et al. [14] compared two types of monocular deprivation: monocular inactivation (MI) and monocular suture (MS). In MI, a drug injection prevents the deprived eye's retina from generating action potentials. In MS,

[1] Note that all authors contributed equally to this paper.

[2] Corresponding author, *E-mail address*: rubin@math.pitt.edu

the retina generates some spontaneous action potentials, and diffuse light entering through the eyelid induces a low level of futher retinal activation. Rittenhouse et al. found that MS creates more of an OD shift in Layer II/III than that which is induced by MI. Since MI more drastically diminishes retinal firing than MS, this result may seem counterintuitive; however, it is consistent with the hypothesis that presynaptic activity, in addition to postsynaptic, is required for OD shift. Computational work has demonstrated previously that spike-timing dependent plasticity (STDP, reviewed e.g. in [3]) can lead to the re-establishment of cortical maps after lesions that wipe out existing maps [18]. In this paper, we show that in a model network, STDP proved to be a highly effective mechanism for inducing both the synaptic *weakening* and *strengthening* components of OD shift. It could not, however, account for the experimental disparity between MS and MI results. We conclude that the corticocortical plasticity observed in MD experiments is unlikely to derive from STDP alone.

Model and Results

We created a neural network consisting of two cortical layers. Our focus on a cortical network was motivated by the fact that Rittenhouse et al. studied animals at a developmental stage in which geniculocortical synapses (to Layer IV neurons) are less plastic than are the highly modifiable corticocortical synapses [12,20,1]. In our model, each of six Layer IV cells and two recurrently connected Layer II/III cells was assigned to an eye, representing two OD columns; see Figure 1b. The structure chosen was based in part on experimental findings that a minority of Layer IV cells project only to II/III cells within the same OD column [2]. Further, while the degree of ocular dominance is only slightly less in cat Layer II/III than in Layer IV in normal conditions [10,20], we assume complete monocularity in Layer IV here to emphasize the differences between different experimental regimes.

All synaptic connections in the model were excitatory and were allowed to evolve via STDP. Changes in synaptic strengths within the model were scaled by multiplicative factors (see [21,15,16]). In particular, in the *heterosynaptic model*, all synapses on one post-synaptic cell compete for a limited pool of trophic factor. Thus, increases in the strength of one synapse onto a cell can limit the possible strengthening of other synapses onto the cell [6]. In the *homosynaptic model*, each synapse has a bound on its strength but bounds on different synapses are independent [4]. The equations in our model are modified from the phenomenological STDP model of Karbowski and Ermentrout [11]. Because we do not expect biophysical details of the spiking properties of the neurons involved to influence the plasticity outcomes under study, each neuron is taken to be a simple phase oscillator, represented by $\theta \in [0, 2\pi)$,

with its firing frequency modulated significantly by Gaussian noise. The phase model on the circle allows for continuous simulation without the reset included in integrate-and-fire models, while still allowing us to pinpoint precise spike times, corresponding to θ reaching 2π from below. When any neuron fires, it induces pulses in an auxiliary variable, s, which serves as a marker for firing time and also drives a slower timing variable u. The combined dynamics of s and u in pre- and postsynaptic cells govern the STDP rule in the model, as shown in Figure 2.

The equations in the model take the following forms. For a Layer IV cell, $\theta' = \omega + \sigma x, \;\; \theta \in [0, 2\pi)$, with default values $\omega = 0.13$, $\sigma = 0.1$, and with x a Wiener process. The value of ω was altered during the course of simulations to emulate responses to visual stimuli. Under *normal* conditions, stimuli were modeled as Markov processes with fixed on and off probabilities. During the duration of a stimulus, ω was switched to 1, leading to rapid spiking. For simplicity, in the normal case, all patterns were assumed to affect all Layer IV cells identically, leading to the same increase in firing rate during the same time period. An example is illustrated in Figure 3 (top). In *monocular inactivation* (MI), Layer IV cells correponding to the inactivated eye did not respond to patterns; moreover, to simulate the elimination of retinal spontaneous activity, we decreased ω to 0.09 in these cells. See Figure 3 (middle). In *monocular suture* (MS), the deprivation of one eye cannot be assumed to be absolute. Thus, Layer IV cells corresponding to the sutured eye fired in response to patterns, but with only a single spike at the end of the pattern [22]; see Figure 3 (bottom).

For a Layer II/III cell, $\theta_i' = \omega_i + \rho \sum_j g_{ji} s_j$, with $\omega_i = 0.01$, to simulate weaker spontaneous firing in Layer II/III than in Layer IV [5,7], with $\rho = 0.3$, and with the sum over cells presynaptic to cell i, with synaptic strengths g_{ji}. The term s_j ensures that the synaptic inputs from a given presynaptic cell are only active for a short time after the cell spikes (see below). Synaptic strengths evolve via $g_{ji}' = \alpha(s_i u_j - \delta s_j u_i) g_{ji} F_{compete}, \;\; i \in \{1, 2\}$ where $\alpha = 0.0001$ and $\delta = 1.5$; see Figure 2. Note that i only takes the values 1 or 2 because only the Layer II/III cells receive synaptic input in the model. In the heterosynaptic case, $F_{compete} = M_i - \sum_j g_{ji}$ to encode competition among all synapses on the same postsynaptic cell; we took $M_i = 2$ independent of i. In the homosynaptic case, $F_{compete} = M_{ji} - g_{ji}$; we took all $M_{ji} = 1.25$. Finally, we set $s_j = \sqrt{\beta} \exp(-\beta(1 - \cos(\theta_j)))$ with $\beta = 75$, such that cell j induces synaptic responses of short duration when θ_j reaches 2π (from below, before wrapping back around to 0), and took $u_j' = -u_j/\mu + s_j$ as a filtered version of s_j. In this equation, $\mu = 3$ except during stimuli, when $\mu = 30$ to smooth out the time course of u_j. The particular parameters selected yield an STDP window of about 20 msec for LTP and LTD from single spike pairs.

As seen in Figure 3, our model produces different firing patterns in normal,

MI, and MS conditions. The experimental manipulations in MI and MS were taken to occur in the eye corresponding to the OD column including cells 1, 3, 4, and 5 (Figure 1b). Initially, g_{31}, g_{51} are strong, corresponding to connections from the Layer IV cells projecting preferentially to cell 1. In the course of each simulation, all weights g_{ji} are free to evolve. Figure 4 illustrates the evolution of synaptic weights g_{31} and g_{61} in each scenario, where g_{61} corresponds to an input to the deprived OD column from the unaltered OD column in the MI and MS cases. Note that the weights are stable in the normal case but that STDP induces a strong shift in the MI and MS cases. While the heterosynaptic model was used here, similar results occurred in the homosynaptic model. Further, results from 20 simulations of each case, for both models, are summarized in Table 1 as mean $\pm$ standard deviation; values below 10^{-4} are denoted by **. These simulations were each run for 200000 time units using XPPAUT [8]. Although in some simulations there appeared to be futher evolution of weights beyond time 200000, the qualitative results and relative levels of the weights appeared to remain consistent beyond this time. Values for g_{31}, g_{61} are shown in bold font to emphasize the OD shift.

A key point to note in Figure 4 is that the weakening of g_{31}, the IV-II/III connection within an OD column, always precedes the strengthening of g_{61}, when an OD shift occurs. The weakening occurs initially because there is a bias toward LTD in the STDP model (e.g. [19]), quantified by the parameter δ. Under normal conditions, bursts of spikes fired by cell 3 in Layer IV in response to stimuli can drive the firing of the Layer II/III cell 1, which compensates for this bias. Once these responses are removed, the firing of cell 3 is mostly uncorrelated from that of cell 1, and the bias toward LTD can take over. Since the Layer IV cell 6 from the nondeprived column still bursts in MI/MS, it gains an advantage at driving cell 1, although this is initially small, because g_{61} is so small. Eventually, this advantage translates into further weakening of g_{31} and strengthening of g_{61}. This rise in g_{61} is consistent with modeling work on the formation of cortical maps [18]. These results do depend on the values of many of the parameters in the model. The value of δ, for example, must be selected appropriately to ensure that weights are stable in normal conditions. Interestingly, however, MD outcomes are essentially invariant under extensive variations in the spontaneous activity rate ω of the Layer IV cells in the deprived column. It appears that the changes driven by elevated firing during visual stimuli, together with trial-to-trial variations due to noise, dominate over the effect of the spontaneous activity rate in shaping the evolution of synaptic weights.

Discussion

STDP has been implicated in visual cortex plasticity [17,9]; however, it has not been modeled previously in the context of OD shift. We found that STDP produces massive OD shifts, as typify monocular deprivation experiments, with both heterosynaptic and homosynaptic bounding mechanisms. STDP alone does not appear to account for differences in OD shift between MI and MS deprivation paradigms, however [14]. This inability to distinguish between MI and MS suggests that other mechanisms, either in conjunction with STDP or on their own, may take part in driving OD shift and particularly in limiting it in MI conditions.

It is theoretically possible that a different form of STDP model, based on multiple spike interactions, would yield different computational results from what we have observed. Moreover, other modeling choices may have affected our findings. Note that we use a simple phase oscillator model, with ω values chosen to speed convergence of our simulations (via a high level of spontaneous activity in Layer IV and a low level of spontaneous activity in Layer II/III, which emphasized the effects of STDP). While preliminary explorations suggest that variations in this particular parameter choice do not alter the qualitative outcomes of our simulations, further study is warranted to explore the effects of other parameters. Further, due to a lack of experimental data, the accuracy of our representations of changes in Layer IV activity in MI and MS conditions is uncertain. Finally, including binocularity in Layer IV may be an important step in limiting remapping in future modeling work.

Acknowledgements

The work of JR was partially supported by NSF grant DMS-0108857. Maureen Ritchey received support as a Center for Neuroscience at University of Pittsburgh Summer Undergraduate Research Fellow.

References

[1] C. Beaver, Q. Ji, and N. Daw. Layer differences in the effect of monocular vision in light- and dark-reared kittens. *Vis. Neurosci.*, **18**:811–820, 2001.

[2] N. Berman, B. Payne, D. Labar, and E. Murphy. Functional organization of neurons in cat striate cortex: variations in ocular dominance and receptive-field type with cortical laminae and location in visual field. *J. Neurophysiol.*, **48**:1362–1377, 1982.

[3] G. Bi. Spatiotemporal specificity of synaptic plasticity: cellular rules and mechanisms. *Biol. Cybern.*, **87**:319–332, 2002.

[4] E. Bienenstock, L. Cooper, and P. Munro. Theory for the development of neuron selectivity: orientation specificity and binocular interaction in visual cortex. *J. Neurosci.*, **2**:32–48, 1982.

[5] J. Brumberg, D. Pinto, and D. Simons. Cortical columnar processing in the rat whisker-to-barrel system. *J. Neurophysiol.*, **82**:1808–1817, 1999.

[6] G. Carmignoto, R. Canella, P. Candeo, M. Cormelli, and L. Maffei. Effects of nerve growth factor on neuronal plasticity of the kitten visual cortex. *J. Physiol.*, **464**:343–360, 1993.

[7] D.Feldmeyer, J. Lubke, A. Silver, and B. Sakmann. Synaptic connections between layer 4 spiny neurone-layer 2/3 pyramidal cell pairs in juvenile rat barrel cortex: physiology and anatomy of interlaminar signalling within cortical columns. *J. Physiol.*, **538**:803–822, 2002.

[8] B. Ermentrout. *Simulating, Analyzing, and Animating Dynamical Systems.* SIAM, Philadelphia, 2002.

[9] R. Froemke and Y. Dan. Spike-timing-dependent synaptic modification induced by natural spike trains. *Nature*, **416**:433–438, 2002.

[10] D. Hubel and T. Wiesel. Receptive fields of cells in striate cortex of very young, visually inexperienced kittens. *J. Neurophysiol.*, **26**:994–1002, 1963.

[11] J. Karbowski and G. Ermentrout. Synchrony arising from a balanced synaptic plasticity in a network of heterogeneous neural oscillators. *Phys. Rev. E*, **65**:0319021–0319025, 2002.

[12] S. Levay, T. Wiesel, and D. Hubel. The development of ocular dominance columns in normal and visually deprived monkeys. *J. Comp. Neurol.*, **191**, 1980.

[13] H. Reiter and M. Stryker. Neural plasticity without postsynaptic action potentials: less-active inputs become dominant when kitten visual cortical cells are pharmacologically inhibited. *Proc. Natl. Acad. Sci. U S A*, **85**:3623–3627, 1988.

[14] C. Rittenhouse, H. Shouval, M. Paradiso, and M. Bear. Monocular deprivation induces homosynaptic long-term depression in visual cortex. *Nature*, **397**:347–350, 1999.

[15] J. Rubin. Steady states in an iterative model for multiplicative spike-timing dependent plasticity. *Network: Comput. Neural Sys.*, **12**:131–140, 2001.

[16] J. Rubin, D. Lee, and H. Sompolinsky. Equilibrium properties of temporally asymmetric Hebbian plasticity. *Phys. Rev. Lett.*, **86**:364–367, 2001.

[17] P. Sjostrom, G. Turrigiano, and S. Nelson. Rate, timing, and cooperativity jointly determine cortical synaptic plasticity. *Neuron*, **32**:1149–1164, 2001.

[18] S. Song and L. Abbott. Cortical development and remapping through spike timing-dependent plasticity. *Neuron*, **13**:339–350, 2001.

[19] S. Song, K. Miller, and L. Abbott. Competitive Hebbian learning through spike-timing-dependent synaptic plasticity. *Nat. Neurosci.*, **3**:919–926, 2000.

[20] J. Trachtenberg, C. Trepel, and M. Stryker. Rapid extragranular plasticity in the absence of thalamocortical plasticity in the developing primary visual cortex. *Science*, **287**:2029–2032, 2000.

[21] M. van Rossum, G. Bi, and G. Turrigiano. Stable Hebbian learning from spike timing-dependent plasticity. *J. Neurosci.*, **20**:8812–8821, 2000.

[22] X. Zhan, C. Cox, J. Rinzel, and S. Sherman. Current clamp and modeling studies of low-threshold calcium spikes in cells of the cat's lateral geniculate nucleus. *J. Neurophysiol.*, **81**:2360–2373, 1999.

Table 1: Asymptotic Weights						
weight	normal (hetero)	MI (hetero)	MS (hetero)	normal (homo)	MI (homo)	MS (homo)
g_{21}	$.0016 \pm .0014$	**	**	$.00030 \pm .00024$	$.00040 \pm .00033$	$.00034 \pm .00033$
g_{31}	$\mathbf{.5764 \pm .2106}$	$\mathbf{.00021 \pm .00032}$	**	$\mathbf{.5573 \pm .2440}$	$\mathbf{.0017 \pm .0016}$	$\mathbf{.00051 \pm .00033}$
g_{41}	$.1180 \pm .0759$	**	**	$.1217 \pm .0942$	$.00016 \pm .00012$	**
g_{51}	$.5250 \pm .2389$	$.00021 \pm .00022$	**	$.5979 \pm .2737$	$.0013 \pm .0010$	$.00092 \pm .00069$
g_{61}	$\mathbf{.0903 \pm .0597}$	$\mathbf{.2740 \pm .3356}$	$\mathbf{.2502 \pm .2629}$	$\mathbf{.1173 \pm .0597}$	$\mathbf{.1332 \pm .1197}$	$\mathbf{.1248 \pm .0617}$
g_{71}	$.1194 \pm .0775$	$.2043 \pm .2459$	$.1939 \pm .2009$	$.1236 \pm .0757$	$.1167 \pm .0775$	$.1615 \pm .1232$
g_{12}	$.0019 \pm .0016$	$.0014 \pm .0019$	$.00091 \pm .00078$	$.00031 \pm .00034$	$.00022 \pm .00020$	$.00028 \pm .00029$
g_{32}	$.1189 \pm .0729$	$.00095 \pm .00101$	$.00057 \pm .00058$	$.1637 \pm .1035$	$.00015 \pm .00011$	$.00010 \pm .00005$
g_{42}	$.0963 \pm .0377$	$.0010 \pm .0011$	$.00057 \pm .00073$	$.1412 \pm .0984$	$.00016 \pm .00011$	**
g_{62}	$.6006 \pm .2630$	$.5747 \pm .3205$	$.6085 \pm .3212$	$.6435 \pm .2149$	$.4753 \pm .2297$	$.8700 \pm .3517$
g_{72}	$.0902 \pm .0485$	$.0876 \pm .0555$	$.1148 \pm .0525$	$.1465 \pm .0911$	$.1294 \pm .1004$	$.1224 \pm .0807$
g_{82}	$.5171 \pm .2109$	$.6786 \pm .3365$	$.6645 \pm .3602$	$.6070 \pm .2061$	$.5772 \pm .1533$	$.5297 \pm .1992$

Figure Captions

Figure 1: a) Diagram of the feline visual system. b) Schematic illustration of the cells in our network model, with lines representing excitatory synaptic connections and line thicknesses corresponding to initial synaptic strengths in simulations.

Figure 2: Cartoon of the phenomenological STDP rule [11]. Solid curves correspond to time course of s, dashed curves to u, for each cell. Left: When a presynaptic cell (j) fires before a postsynaptic one (i), s_i, u_j line up to give LTP (dotted line). Right: When a presynaptic cell fires after a postsynaptic one, s_j, u_i line up to give LTD (dotted line).

Figure 3: Example firing patterns in normal (top), MI (middle), and MS (bottom) scenarios. θ is plotted on $[0, 2\pi)$, so that when θ reaches 2π, a spike occurs and θ wraps around to 0 (with no jump in θ').

Figure 4: Evolution of synaptic weights. The heterosynaptic synaptic bounding model was used here. Note the different timescales in different plots. a) Normal conditions. The solid curve corresponds to g_{31}, the weight of a synapse within an OD column, while the dashed curve corresponds to g_{61}, the weight of a synapse across OD columns. b) MI conditions. c) MS conditions. In b),c), g_{31} connects cells within the deprived column.

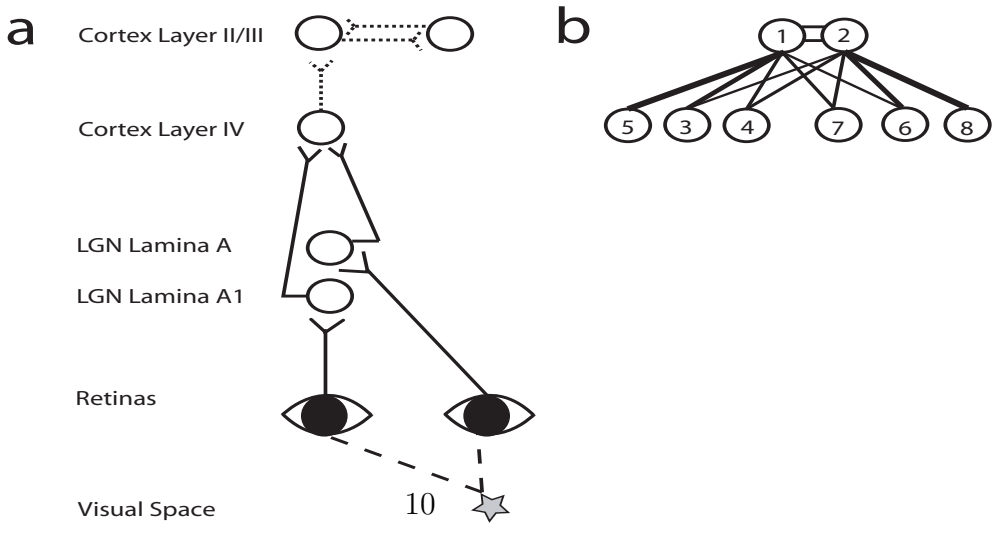
a
Cortex Layer II/III
Cortex Layer IV
LGN Lamina A
LGN Lamina A1
Retinas
Visual Space
b
1
2
5
3
4
7
6
8

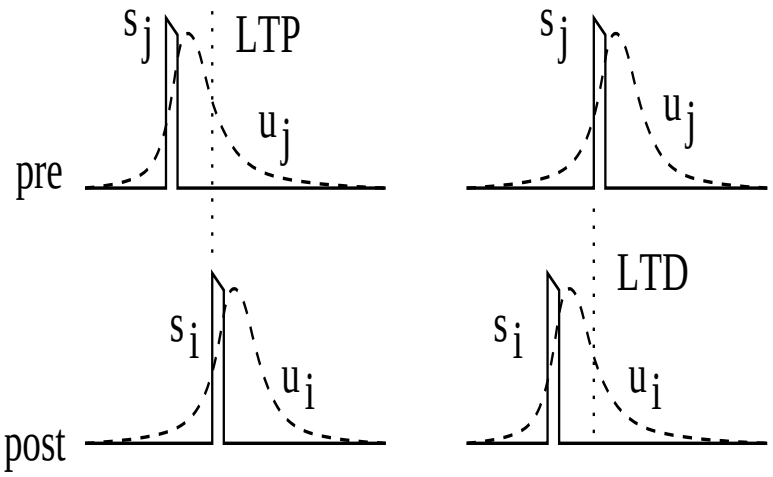

Figure 2

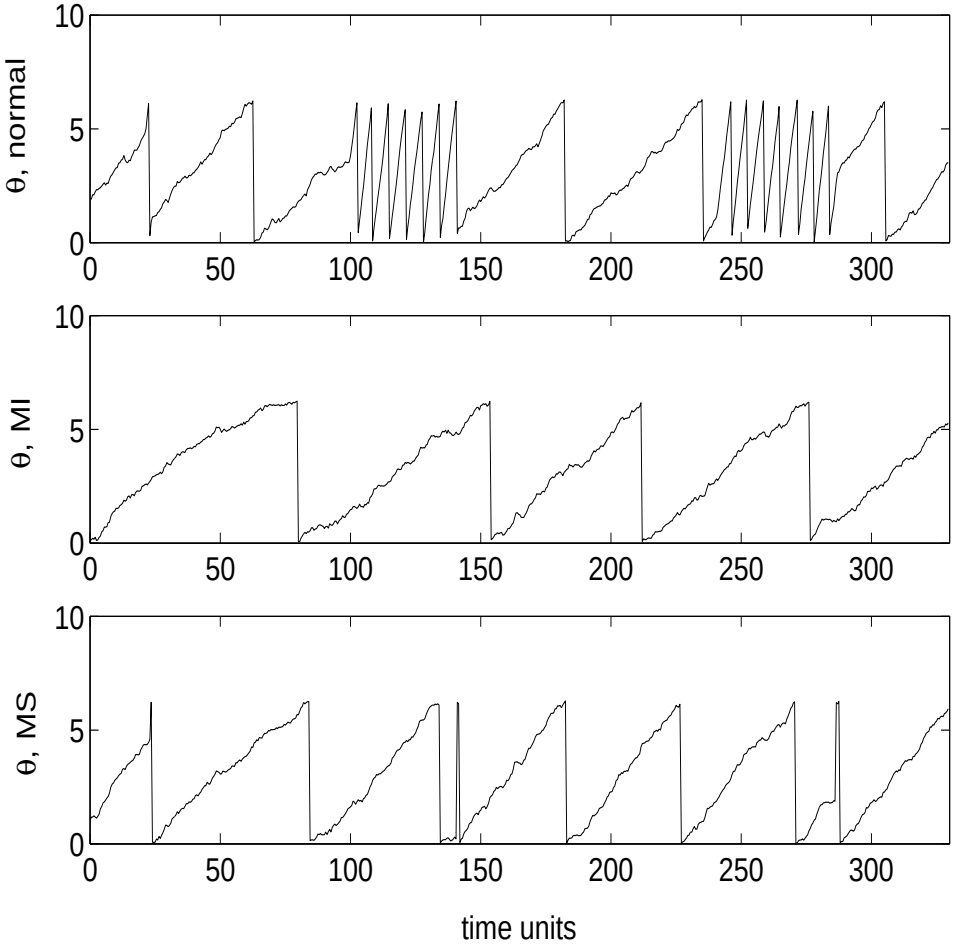

Figure 3

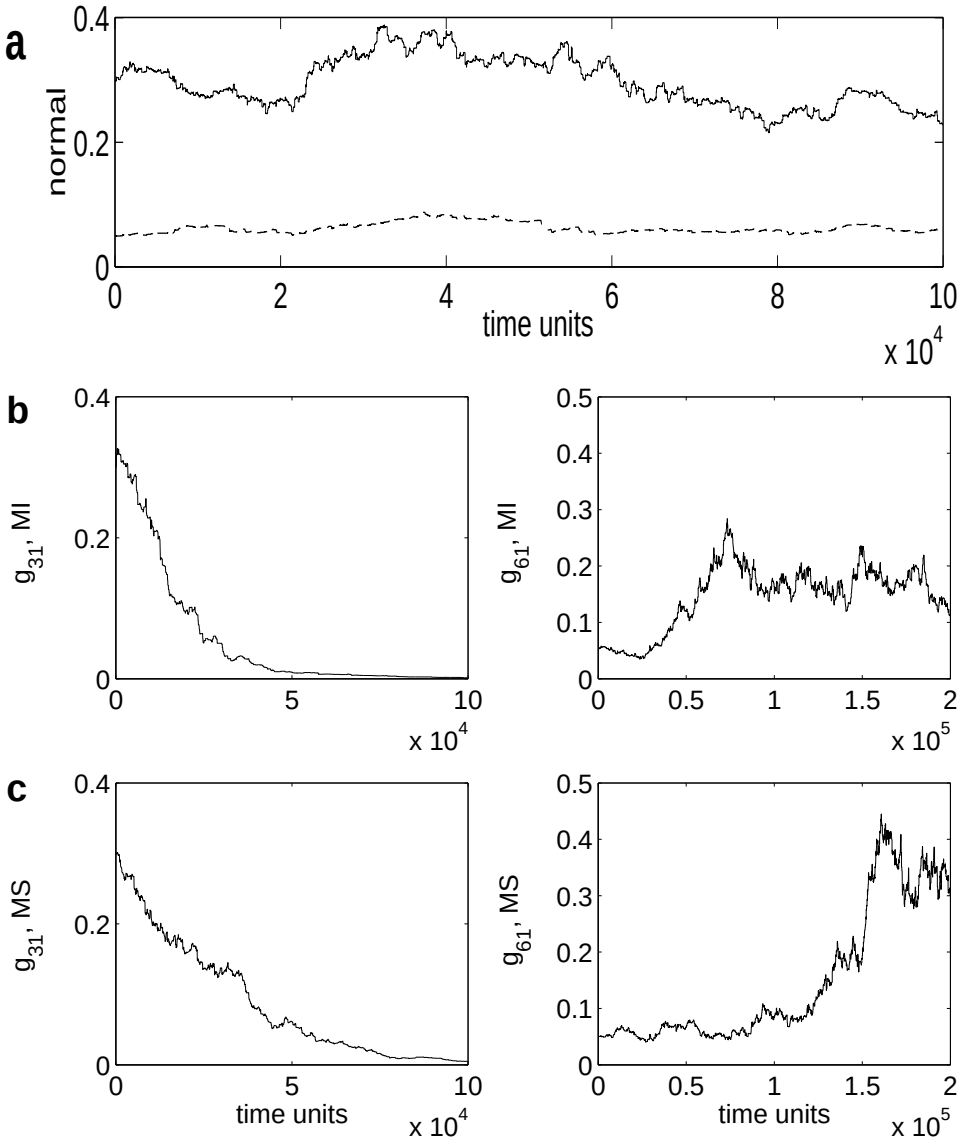
a
normal
0.4
0.2
0
0
2
4
6
8
10
time units
x 10^4
b
g31, MI
0.4
0.2
0
0
5
10
x 10^4
g61, MI
0.5
0.4
0.3
0.2
0.1
0
0
0.5
1
1.5
2
x 10^5
c
g31, MS
0.4
0.2
0
0
5
10
time units
x 10^4
g61, MS
0.5
0.4
0.3
0.2
0.1
0
0
0.5
1
1.5
2
time units
x 10^5